Draft version August 6, 2018
Typeset using LaTeX **twocolumn** style in AASTeX61

THERMONUCLEAR REACTION RATES FOR TRITIUM + DEUTERIUM FUSION USING BAYESIAN METHODS

Christian Iliadis,[1,2] Rafael S. de Souza,[1] S. Reece Boston,[1] and Alain Coc[3]

[1] *Department of Physics & Astronomy, University of North Carolina at Chapel Hill, NC 27599-3255, USA*
[2] *Triangle Universities Nuclear Laboratory (TUNL), Durham, North Carolina 27708, USA*
[3] *Centre de Sciences Nucléaires et de Sciences de la Matière, Univ. Paris-Sud, CNRS/IN2P3, Université Paris-Saclay, Bâtiment, 104, F-91405 Orsay Campus, France*

(Received August 6, 2018)

Submitted to ApJ

ABSTRACT

The ^{3}H(d,n)^{4}He reaction has a large low-energy cross section and will likely be used in future commercial fusion reactors. It also takes place in big bang nucleosynthesis. Studies of both scenarios require accurate and precise thermonuclear reaction rates. To this end, we implement a one-level, two-channel R-matrix approximation into a Bayesian model. Our main goals are to predict reliable astrophysical S-factors and to estimate R-matrix parameters using the Bayesian approach. All relevant parameters are sampled in our study, including the channel radii, boundary condition parameters, and data set normalization factors. In addition, we take uncertainties in both measured bombarding energies and S-factors into account. Thermonuclear rates of the ^{3}H(d,n)^{4}He reaction are derived by numerically integrating the Bayesian S-factor samples. The present rate uncertainties at temperatures between 1 MK and 1 GK are in the range of 1.1% to 1.5%. Our reaction rates differ from previous results by up to 2.5%. The present rate uncertainties are also larger, but more reliable, compared to previous studies that did not include the channel radii, boundary condition parameters, and data set normalization factors in the fitting. Finally, we investigate previous claims of electron screening effects in the published ^{3}H(d,n)^{4}He data. No such effects are evident and only an upper limit for the electron screening potential can be obtained.

Corresponding author: Christian Iliadis
iliadis@unc.edu

1. INTRODUCTION

The cross section of the ^{3}H(d,n)^{4}He reaction has a large Q-value of 17.6 MeV, and a large cross section that peaks at $\approx$ 5 barn near a deuteron (triton) bombarding energy of 105 keV (164 keV). For these reasons, the ^{3}H(d,n)^{4}He reaction will most likely fuel the first magnetic and inertial confinement fusion reactors for commercial energy production (Wilson et al. 2008; Kim et al. 2012). The reactors are expected to operate in the thermal energy range of kT= 1 $-$ 30 keV, corresponding to temperatures of T= 12 $-$ 350 MK. These values translate to kinetic energies between 4 keV and 120 keV in the ^{3}H + d center-of-mass system, which can be compared with a height of $\approx$280 keV for the Coulomb barrier. The ^{3}H(d,n)^{4}He reaction also occurs during big bang nucleosynthesis, at temperatures between 0.5 GK and 1.0 MK, corresponding to center-of-mass Gamow peak energies in the range of 13 $-$ 252 keV.

The ^{3}H + d low-energy cross section is dominated by a s-wave resonance with a spin-parity of $J^\pi = 3/2^+$, corresponding to the second excited level near $E_x \approx$ 16.7 MeV excitation energy in the ^{5}He compound nucleus (Tilley et al. 2002). This level decays via emission of d-wave neutrons. It has mainly a ^{3}H + d structure, corresponding to a large deuteron spectroscopic factor (Barker 1997), while shell model calculations predict a relatively small neutron spectrocopic factor (Barker & Woods 1985). However, the neutron penetrability is much larger than the deuteron penetrability at these low energies, so that incidentally the partial widths for the deuteron and neutron channel (Γ_d, Γ_n), given by the product of spectroscopic factor and penetrability, become similar in magnitude. This near equality of the deuteron and neutron partial widths causes the large low-energy cross section of the ^{3}H(d,n)^{4}He reaction (Conner et al. 1952; Argo et al. 1952) since, considering a simple Breit-Wigner expression, the cross section maximum is proportional to $\Gamma_d\Gamma_n/(\Gamma_d+\Gamma_n)^2$, which peaks for the condition $\Gamma_d \approx \Gamma_n$.

For the design of fusion reactors and for purposes of plasma diagnostics, it is important to know the ^{3}H(d,n)^{4}He thermonuclear rate with the greatest possible accuracy. Different strategies to analyze the data have been adopted previously. Fits of the available ^{3}H(d,n)^{4}He data using Breit-Wigner expressions were reported by Duane (1972) and Angulo et al. (1999), while a Padé expansion was used in Peres (1979). Single-level and multi-level R-matrix fits to ^{3}H(d,n)^{4}He data were discussed by Jarmie et al. (1984); Brown et al. (1987); Barker (1997); Descouvemont et al. (2004). A comprehensive R-matrix approach that in addition to the ^{3}H(d,n)^{4}He data included elastic and inelastic cross sections of the ^{3}H + d and ^{4}He + n systems, and incorporated 2664 data points and 117 free parameters, was presented by Hale, Brown & Jarmie (1987); Bosch & Hale (1992). An analysis of ^{3}H(d,n)^{4}He data using effective field theory, with only three fitting parameters, can be found in Brown & Hale (2014).

In the present work, our first goal is to quantify the uncertainties in the thermonuclear rates (or reactivities) of the ^{3}H(d,n)^{4}He reaction. All previous works employed traditional (i.e., frequentist) statistics in the data fitting, assuming Gaussian likelihoods throughout the analysis, and disregarding any uncertainties in the center-of-mass energies. Here, we will discuss an analysis using Bayesian techniques. Such a study, for the analog ^{3}He(d,p)^{4}He reaction, has been published recently by de Souza et al. (2018). The Bayesian approach has major advantages, as discussed by Iliadis et al. (2016); Gómez Iñesta et al. (2017), because it is not restricted to Gaussian likelihoods, but instead allows for implementing into the model the likelihoods that best apply to the problem at hand. Also, all previous R-matrix analyses kept the channel radii and boundary condition parameters constant during the fitting. In reality, these quantities are not sharply constrained, and thus our limited knowledge will impact the uncertainties of the derived S-factors and thermonuclear rates. Furthermore, uncertainties affect not only the S-factors, but also the center-of-mass energies. Uncertainties in both the independent and dependent variables can be easily implemented into a Bayesian model, whereas no simple prescription for such a procedure exists in traditional statistics. Our second goal is to investigate the usefulness of the Bayesian approach for estimating the R-matrix parameters. The results will prove useful in future studies that involve multiple channels and resonances.

In Section 2, we briefly present the S-factor data adopted in the present work. Section 3 summarizes the reaction formalism. Our Bayesian model for fitting the S-factor data is discussed in Section 4, including likelihoods, model parameters, and priors. The data analysis is discussed in Section 5. In Section 6, we present Bayesian thermonuclear reaction rates. A summary and conclusions are given in Section 7. Our Bayesian model is summarized in Apendix A, and an evaluation of the data adopted in our analysis is presented in Appendix B.

2. DATA SELECTION

Several previous works have indiscriminately used all available ^{3}H + d cross section data in the fitting. A rigorous data analysis requires a careful distinction between statistical and systematic uncertainties (Section 4.2), because we need to implement these effects

separately in our Bayesian model. For this reason, we will consider only those experiments for which we can quantify the two contributions separately. Detailed information regarding the experimental uncertainties is provided in Appendix B.

The ^{3}H(d,n)^{4}He low-energy cross section represents a steep function of energy. For example, at 20 keV in the center of mass, an energy variation of only 0.1 keV causes a 2% change in cross section, while at 10 keV a variation of 0.1 keV causes a 6% change in the cross section. Therefore, accurate knowledge of the incident beam energy becomes crucial for predicting cross sections and thermonuclear rates. Experiments that employed thin targets will be less prone to systemic effects than those using thick targets. For example, consider the data measured by Argo et al. (1952), which were adopted at face value in previous thermonuclear rate determinations. Argo et al. (1952) employed 1.5 mg/cm^2 thick aluminum entrance foils for their deuterium gas target. Under such conditions, tritons that slowed down to a laboratory energy of 183 keV after passing the entrance foil would have lost 568 keV in the foil, giving rise to an overall beam straggling of about 31 keV. In this case, it is difficult to reliably correct the cross section for the beam energy loss. Compare this situation to the measurement by Jarmie et al. (1984), where the triton beam lost an energy less than 200 eV while traversing a windowless deuterium gas target. A detailed discussion of all data sets that have been adopted or disregarded in the present analysis is given in Appendix B.

All of our adopted data are shown in Figure 1. They originated from the experiments by Conner et al. (1952); Arnold et al. (1953); Kobzev et al. (1966); Jarmie et al. (1984); Brown et al. (1987), and contain 191 data points in the center-of-mass energy region between 5 keV and 270 keV. Notice that the results of Brown et al. (1987) have been used at face value in previous thermonuclear rate estimations, although these authors did not determine any absolute cross sections. In Section 5.2 we will discuss how to implement such data into the Bayesian model.

3. REACTION FORMALISM

Since we are mainly interested in the low-energy region, where the $3/2^+$ s-wave resonance dominates the cross section, we will describe the theoretical energy dependence of the cross section using a one-level, two-channel R-matrix approximation. This assumption is justified by previous works that found that the measured S-factor data are about equally well reproduced by single-level and multi-level R-matrix analyses at center-of-mass energies below ≈ 100 keV (see, e.g., Figure 4 in Hale, Brown & Paris (2014)).

The integrated cross section of the ^{3}He(d,n)^{4}He reaction is given by

$$\sigma_{dn}(E) = \frac{\pi}{k^2}\frac{2J+1}{(2j_1+1)(2j_2+1)}\,|S_{dn}|^2 \qquad (1)$$

where k and E are the wave number and energy, respectively, in the ^{3}H + d center-of-mass system, $J = 3/2$ is the resonance spin, $j_1 = 1/2$ and $j_2 = 1$ are the spins of the triton and deuteron, respectively, and S_{dn} is the scattering matrix element. The corresponding astrophysical S-factor is defined by

$$S_{bare}(E) \equiv E e^{2\pi\eta}\sigma_{dn}(E) \qquad (2)$$

where η is the Sommerfeld parameter. The scattering matrix element can be expressed as (Lane & Thomas 1958)

$$|S_{dn}|^2 = \frac{\Gamma_d\Gamma_n}{(E_0+\Delta-E)^2+(\Gamma/2)^2} \qquad (3)$$

where E_0 denotes the level eigenenergy. The partial widths of the ^{3}H + d and ^{4}He + n channels (Γ_d, Γ_n), the total width (Γ), and total level shift (Δ), which are all energy dependent, are given by

$$\Gamma = \sum_c \Gamma_c = \Gamma_d + \Gamma_n\ , \quad \Gamma_c = 2\gamma_c^2 P_c \qquad (4)$$

$$\Delta = \sum_c \Delta_c = \Delta_d + \Delta_n\ , \quad \Delta_c = -\gamma_c^2(S_c - B_c) \qquad (5)$$

where γ_c^2 is the reduced width, and B_c is the boundary condition parameter. The energy-dependent quantities P_c and S_c denote the penetration factor and shift factor, respectively, for channel c (either d + ^{3}H or n + ^{4}He). They are computed numerically from the Coulomb wave functions, F_ℓ and G_ℓ, according to

$$P_c = \frac{ka_c}{F_\ell^2+G_\ell^2}\ , \quad S_c = \frac{ka_c(F_\ell F_\ell' + G_\ell G_\ell')}{F_\ell^2+G_\ell^2} \qquad (6)$$

The Coulomb wave functions and their radial derivatives are evaluated at the channel radius, a_c; the quantity ℓ denotes the orbital angular momentum for a given channel.

In some cases, the fit to the data can be improved by adding a distant level in the analysis, located at a fixed energy outside the range of interest. However, such "background poles" have no physical meaning. As will become apparent below, the single-level, two-channel approximation represents a satisfactory model for the low-energy data of interest here.

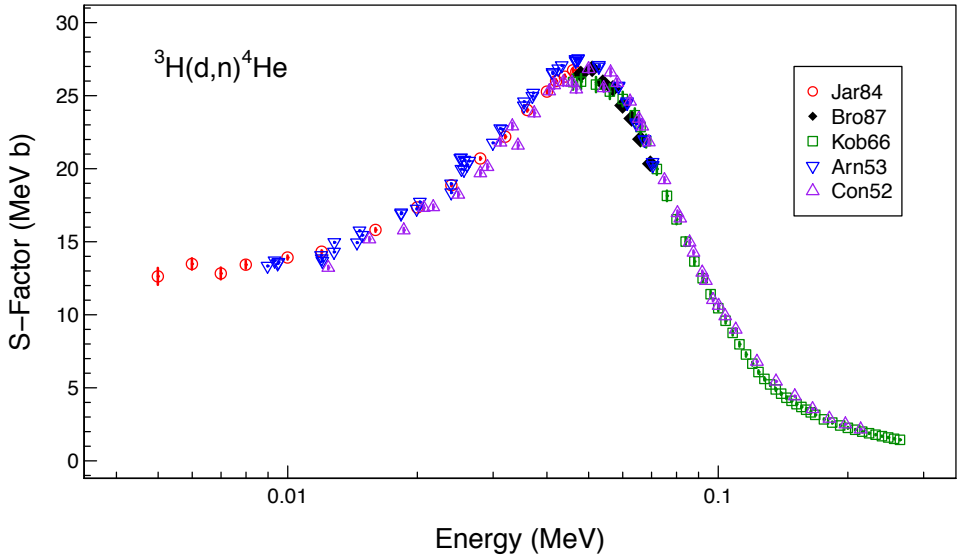

Figure 1. The data used in our analysis: (Red circles) Jarmie et al. (1984); (Black diamonds) Brown et al. (1987); (Green squares) Kobzev et al. (1966); (Blue triangles) Arnold et al. (1953); (Purple triangles) Conner et al. (1952). Absolute cross sections were not determined in Brown et al. (1987) and their data were normalized to those of Jarmie et al. (1984). Only statistical uncertainties are shown, but for many of the data points they are smaller than the symbol sizes. Details regarding the data evaluation are given in the appendix. The energy ranges important for fusion reactors and big bang nucleosynthesis are $4 - 120$ keV and $13 - 252$ keV, respectively.

Teichmann & Wigner (1952) showed that the reduced width, $\gamma^2_{\lambda c}$, of an eigenstate λ cannot exceed, *on average*, the single-particle limit, given by

$$\langle \gamma^2_{\lambda c} \rangle \lesssim \frac{3}{2} \frac{\hbar^2}{m_c a_c^2} \tag{7}$$

where m_c is the reduced mass of the interacting pair of particles in channel c. In this original formulation, Equation 7 only holds for a reduced width that is averaged over many eigenstates λ. Using the actual strength of the residual interaction in nuclei, Dover, Mahaux & Weidenmüller (1969) found a single-particle limit of

$$\gamma^2_{\lambda c} \lesssim \frac{\hbar^2}{m_c a_c^2} \tag{8}$$

for an individual resonance in a nucleon channel. The quantity $\gamma^2_{WL} \equiv \hbar^2/(m_c a_c^2)$ is often referred to as the Wigner limit. Considering the various assumptions made in deriving the above expressions, the Wigner limit provides only an approximation for the maximum value of a reduced width. The Wigner limit can also be used to define a "dimensionless reduced width", $\theta^2_{\lambda c}$, according to

$$\gamma^2_{\lambda c} \equiv \frac{\hbar^2}{m_c a_c^2} \theta^2_{\lambda c} \tag{9}$$

We perform the S-factor fit to the data using the expression (Assenbaum, Langanke & Rolfs 1987; Engstler et al. 1988)

$$S(E) \approx S_{bare}(E) e^{\pi \eta (U_e/E)} \tag{10}$$

where U_e is the energy-independent electron screening potential. The latter quantity has a positive value and depends on the identities of target and projectile, i.e., it differs for forward and inverse kinematics experiments.

R-matrix parameters and cross sections derived from data have a well-known dependence on the channel (or interaction) radius, which is usually expressed as

$$a_c = r_0 \left(A_1^{1/3} + A_2^{1/3} \right) \tag{11}$$

where A_i are the mass numbers of the interacting nuclei, and r_0 is the radius parameter, with a value usually chosen between 1.4 fm and 1.5 fm. The channel radius dependence arises from the truncation of the R-matrix to a restricted number of poles (i.e., a finite set of eigenenergies). The radius of a given channel has no rigorous physical meaning, except that the chosen value should exceed the sum of the radii of the colliding nuclei (see, e.g., Descouvemont & Baye (2010), and references therein). The radius dependence can likely be reduced by including more levels (including background poles) in the data analysis, but only at the cost of increasing the number of fitting parameters. In any case, it is important to include the effects of varying the channel radius in the data analysis. We will return to this issue in Section 5.

Another issue that needs investigating is the effect of the arbitrary choice of the boundary condition parameter, B_c. It can be seen from Equations 3 and 5 that changing B_c will result in a corresponding change of the

eigenenergy, E_0, to reproduce the measured location of the cross section maximum. Lane & Thomas (1958) recommended to chose B_c in the one-level approximation so that the eigenvalue E_0 lies within the width of the observed resonance. For a relatively narrow resonance, one can assume that the maximum of the scattering matrix element (Equation 3) occurs at an energy, E_r, defined by $E_0 + \Delta(E_r) - E_r = 0$. In that case, the customary choice for the boundary condition parameter is $B_c = S_c(E_r)$. This choice results in $\Delta(E_r) = 0$, or $E_r = E_0$, in agreement with the recommendation of Lane & Thomas (1958). As will be discussed in Section 5, the situation is not so obvious in the case of the exceptionally broad low-energy resonance in ^{3}H(d,n)^{4}He.

4. BAYESIAN MODELS

4.1. *General Aspects*

We analyze the S-factor data using Bayesian statistics and Markov chain Monte Carlo (MCMC) algorithms. The application of this method to nuclear astrophysics has been discussed in Iliadis et al. (2016) and Gómez Iñesta et al. (2017). Bayes' theorem is given by (Jaynes & Bretthorst 2003)

$$p(\theta|y) = \frac{\mathcal{L}(y|\theta)\pi(\theta)}{\int \mathcal{L}(y|\theta)\pi(\theta)d\theta} \tag{12}$$

where the data are denoted by y and the complete set of model parameters is described by the vector θ. All factors entering in Equation 12 represent probability densities: $\mathcal{L}(y|\theta)$ is the likelihood, i.e., the probability that the data, y, were obtained assuming given values of the model parameters; $\pi(\theta)$ is called the prior, which represents our state of knowledge about each parameter before seeing the data; the product of likelihood and prior defines the posterior, $p(\theta|y)$, i.e., the probability of the values of a specific set of model parameters given the data; the denominator, called the evidence, is a normalization factor and is not important in the context of the present work. It can be seen from Equation 12 that the posterior represents an update of our prior state of knowledge about the model parameters once new data become available.

The random sampling of the posterior is usually performed numerically over many parameter dimensions using MCMC algorithms (Metropolis et al. 1953; Hastings 1970; Geyer 2011). A Markov chain is a random walk, where a transition from state i to state j is independent (memory-less) of how state i was populated. The fundamental theorem of Markov chains states that for a very long random walk the proportion of time (i.e., the probability) the chain spends in some state j is independent of the initial state it started from. This set of limiting, long random walk, probabilities is called the stationary (or equilibrium) distribution of the Markov chain. When a Markov chain is constructed with a stationary distribution equal to the posterior, $p(\theta|y)$, the samples drawn at every step during a sufficiently long random walk will closely approximate the posterior density. Several related algorithms (e.g., Metropolis, Metropolis-Hastings, Gibbs) are known to solve this problem numerically. The combination of Bayes theorem and MCMC algorithms allows for computing models that are too difficult to estimate using traditional statistical methods.

In this work we employ the program JAGS ("Just Another Gibbs Sampler") for the analysis of Bayesian models using MCMC sampling (Plummer 2003). Specifically, we will employ the rjags package that works directly with JAGS within the R language (R Core Team 2015). Running a JAGS model refers to generating random samples from the posterior distribution of model parameters. This involves the definition of the model, likelihood, and priors, as well as the initialization, adaptation, and monitoring of the Markov chain.

4.2. *Types of uncertainties*

Of particular interest for the present work is the concept of a hierarchical Bayesian model (Hilbe, de Souza & Ishida 2017, and references therein). It allows us to take all relevant effects and processes into account that affect the measured data, which is often not possible with traditional statistics. We first need to define the different types of uncertainties impacting both the measured energy and S-factor in a nuclear physics experiment.

Statistical (or *random*) uncertainties usually follow a known probability distribution. When a series of independent experiments is performed, statistical uncertainties will give rise to different results in each individual measurement. Statistical uncertainties can frequently be reduced by improving the data collection procedure or by collecting more data. They have a number of different causes. For example, for the S-factor, one source is the Poisson uncertainty, which derives from measuring N counts with an associated uncertainty of $\sqrt{N}$. Another source is caused by the background that needs to be subtracted from the measured total intensity to find the net intensity of the signal. A third source is introduced by the detector, which is subject to additional random uncertainties (e.g., corrections for detection efficiencies). The cumulative effect causes the measured number of signal counts to fluctuate randomly from data point to data point.

Systematic uncertainties originate from sources that systematically shift the signal of interest either too high or too low. They do not usually signal their existence

by a larger fluctuation of the data, and they are not reduced by combining the results from different measurements or by collecting more data. When the experiment is repeated, the presence of systematic effects may not produce different answers. Reported systematic uncertainties are at least partially based on assumptions made by the experimenter, are model-dependent, and follow vaguely known probability distributions (Heinrich & Lyons 2007). In a nuclear physics experiment, systematic effects impact the overall normalization by shifting all points of a given data set into the same direction. They are correlated from data point to data point, in the sense that if one happened to know how to correct such an uncertainty for one data point, then one could calculate the correction for the other data points as well.

In many cases, the scatter about the best-fit model is larger than can be explained by the reported measurement uncertainties. It its useful in such situations to introduce an *intrinsic* uncertainty (or *intrinsic scatter*), which describes additional sources of uncertainty in the data that were not properly accounted for by the experimenter. For example, the reported statistical uncertainties may have been too optimistic because target thickness or ion beam straggling effects were underestimated; or perhaps systematic effects that impact data points *differently* in a given experiment were unknown to the experimenter.

To summarize, we assume that three independent effects impact the measured energies and S-factors: (i) statistical uncertainties, which perturb the true (but unknown) energy or S-factor by an amount of ϵ_{stat}; (ii) systematic uncertainties, which perturb the energy or S-factor by an amount of ϵ_{syst}; and (iii) intrinsic scatter, which perturbs the energy or S-factor by an amount of ϵ_{intr}. The overall goal is to estimate credible values for the true energy and S-factor based on the measured data.

4.3. *Likelihoods and Priors*

In this section, for illustrative purposes, we will explain how to construct a hierarchical Bayesian model by focussing on uncertainties in the dependent variable, i.e., the S-factor. Our full Bayesian model, including uncertainties in both energy and S-factor, will be discussed in a later section.

Suppose first that the experimental S-factor, S^{exp}, is subject to experimental statistical uncertainties only ($\epsilon_{intr} = \epsilon_{syst} = 0$; $\epsilon_{stat} \neq 0$). Then the likelihood is given by

$$\mathcal{L}(S^{exp}|\theta) = \prod_{i=1}^{N} \frac{1}{\sigma_{stat,i}\sqrt{2\pi}} e^{-\frac{[S_i^{exp} - S(\theta)_i]^2}{2\sigma^2_{stat,i}}} \tag{13}$$

where $S(\theta)_i$ is the model S-factor (e.g., obtained from R-matrix theory); the product runs over all data points, labeled by i. The likelihood represents a product of normal distributions, each with a mean of $S(\theta)_i$ and a standard deviation of $\sigma_{stat,i}$, given by the experimental statistical uncertainty of datum i. In symbolic notation, the above expression can be abbreviated by

$$S_i^{exp} \sim N(S(\theta)_i, \sigma^2_{stat,i}) \tag{14}$$

where N denotes a normal probability density, and the symbol "$\sim$" stands for "sampled from." If, on the other hand, only intrinsic uncertainties impact the S-factor data ($\epsilon_{syst} = \epsilon_{stat} = 0$; $\epsilon_{intr} \neq 0$), and we assume that these follow a normal probability distribution with a standard deviation of σ_{intr}, the likelihood can be written as

$$\mathcal{L}(S^{exp}|\theta) = \prod_{i=1}^{N} \frac{1}{\sigma_{intr}\sqrt{2\pi}} e^{-\frac{[S_i^{exp} - S(\theta)_i]^2}{2\sigma^2_{intr}}} \tag{15}$$

In symbolic notation, we obtain

$$S_i^{exp} \sim N(S(\theta)_i, \sigma^2_{intr}) \tag{16}$$

When both effects are taken simultaneously into account ($\epsilon_{intr} \neq 0$; $\epsilon_{stat} \neq 0$), the overall likelihood is given by a nested (and cumbersome explicit) expression. In the convenient symbolic notation, we can write

$$S'_i \sim N(S(\theta)_i, \sigma^2_{stat,i}) \tag{17}$$

$$S_i^{exp} \sim N(S'_i, \sigma^2_{intr}) \tag{18}$$

These two expressions show in an intuitive manner how the overall likelihood is constructed: first, statistical uncertainties, quantified by the standard deviation $\sigma_{stat,i}$ of a normal probability density, perturb the true (but unknown) value of the S-factor at energy i, $S(\theta)_i$, to produce a value of S'_i; second, the latter value is perturbed, in turn, by the intrinsic uncertainty, quantified by the standard deviation σ_{intr} of a normal probability density, to produce the measured value of S_i^{exp}.

The above discussion demonstrates how any effect impacting the data can be implemented in a straightforward manner into a Bayesian data analysis. There is nothing special about adopting normal distributions in the example above, which we only chose to explain a complex problem in simple words. As will be seen below, some of the likelihood functions used in the present work are non-normal.

Each of the model parameters, contained in the vector θ, requires a prior distribution. It contains the information on the probability density of a given parameter prior to analyzing the data under consideration. For example,

if our model has only one parameter, and if all we know is that the value of a parameter, θ, lies somewhere in a region from zero to θ_{max}, we can write in symbolical notation for the prior

$$\theta \sim U(0, \theta_{max}) \tag{19}$$

where U denotes a uniform probability density.

Normalization factors related to systematic uncertainties represent a special case. For example, a systematic uncertainty of, say, $\pm 5\%$, implies that the systematic factor uncertainty is 1.05. The true value of the normalization factor, f, is unknown at this stage, otherwise there would be no systematic uncertainty. However, we do have one piece of information: the expectation value of the normalization factor is unity. If this would not be the case, we would have corrected the data for the systematic effect.

A useful distribution for normalization factors is the lognormal probability density, which is characterized by two quantities, the location parameter, μ, and the spread parameter, σ. The median value of the lognormal distribution is given by $x_{med} = e^{\mu}$, while the factor uncertainty, for a coverage probability of 68%, is $f.u. = e^{\sigma}$. We will include in our Bayesian model a systematic effect on the S-factor as an informative, lognormal prior with a median of $x_{med} = 1.0$, or $\mu = \ln x_{med} = 0$, and a factor uncertainty given by the systematic uncertainty, i.e., in the above example, $f.u. = 1.05$, or $\sigma = \ln f.u. = \ln(1.05)$. The prior is explicitly given by

$$\pi(f_n) = \frac{1}{\ln(f.u.)_n \sqrt{2\pi} f_n} e^{-\frac{(\ln f_n)^2}{2[\ln(f.u.)_n]^2}} \tag{20}$$

where the subscript n labels the different data sets. We write in symbolic notation

$$f_n \sim LN(0, [\ln(f.u.)_n]^2) \tag{21}$$

where LN denotes a lognormal probability density. For more information on this choice of prior, see Iliadis et al. (2016).

In the present work, we employ for a given parameter a prior that best reflects the physics involved. Depending on the parameter, we use as priors uniform distributions, broad normal densities truncated at zero, narrow normal densities, and log-normal densities.

5. DATA ANALYSIS

5.1. *Results with all parameter values fixed*

Although the ^{3}H(d,n)^{4}He cross section is dominated at low energies by only a single resonance, any fitting procedure will face a number of interesting problems.

First, Argo et al. (1952) noted that, as is usual when fitting a resonance curve to data, an equally good fit is obtained for two possible solutions of the partial width ratio ($\Gamma_d/\Gamma_n > 1$ or < 1), and that it is not possible to chose between them without additional information about the magnitude of the reduced widths γ_d^2 and γ_n^2. They also note, however, that the two solutions do not give widely different parameter values since the Γ_d/Γ_n ratio is of order unity.

Second, in addition to the ambiguity introduced by the ratio of partial withs, there is another complication related to their absolute magnitude. Consider the two S-factor parameterizations shown in Figure 2, where the data are the same as in Figure 1. The blue curve was obtained using the best-fit values of Barker (1997) for the eigenenergy and the reduced widths ($E_0 = 0.0912$ MeV, $\gamma_d^2 = 2.93$ MeV, $\gamma_n^2 = 0.0794$ MeV); Barker's choices for the channel radii and boundary condition parameters were $a_d = 6.0$ fm, $a_n = 5.0$ fm, $B_d = -0.285$, $B_n = -0.197$. Barker's derived deuteron reduced width exceeds the Wigner limit by a factor of three, which emphasizes the exceptional character of the low-energy resonance. Although the data analyzed by Barker and the data evaluated in the present work (see Appendix B) are not identical, it can be seen that his best-fit curve describes the observations well. The red curve was computed by arbitrarily multiplying Barker's reduced width values by a factor of 10 ($\gamma_d^2 = 29.3$ MeV, $\gamma_n^2 = 0.794$ MeV) and slightly adjusting the eigenenergy and boundary condition parameter ($E_0 = 0.102$ MeV, $B_d = -0.267$). Notice that the red curve does not represent any best-fit result, but its sole purpose is to demonstrate that similar S-factors can be obtained by vastly different values of the partial widths. However, the red curve represents an unphysical result if we consider additional constraints: a deuteron reduced width of $\gamma_d^2 = 29.3$ MeV, obtained with a channel radius of $a_d = 6.0$ fm, exceeds the Wigner limit (Equation 8) by a factor of 30 and is thus highly unlikely.

The latter ambiguity is caused by the structure of Equation 3. The large reduced width of the deuteron channel dominates the level shift (Equation 5) and also the factor $(E_0 + \Delta - E)$ in Equation 3. Therefore, if the reduced or partial widths for both channels are multiplied by a similar factor, the shape and magnitude of the S-factor is only slightly changed. This ambiguity in the parameter selection cannot be removed even when $d + t$ elastic scattering data are simultaneously analyzed together with the reaction data, as noted by Barit & Sergeev (1971).

Third, the large total width of the resonance is similar in magnitude to the resonance energy. The resonance is

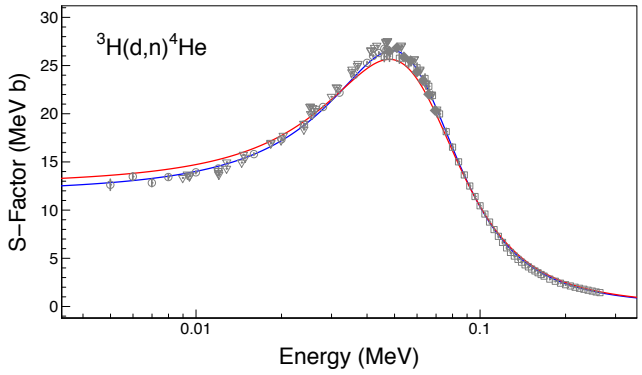

Figure 2. Astrophysical S-factors computed using the single-level, two-channel approximation (Equations 1 − 3). The data are the same as in Figure 1. The blue curve is computed with the best-fit parameter values of Barker (1997). The red curve is obtained by arbitrarily multiplying Barker's reduced widths by a factor of 10 and adjusting the eigenenergy and boundary condition parameter slightly. The red curve does not represent any best-fit result and serves for illustrative purposes only.

so broad that the experimental values of the scattering matrix element, $|S_{dn}|^2$, the cross section, σ, and the S-factor, $S_{bare}(E)$, peak at markedly different center-of-mass energies (≈80 keV, ≈65 keV, and ≈50 keV, respectively). The differences are caused by the energy dependences of the wave number ($k^2 \sim E$) in Equation 1 and the Gamow factor ($e^{2\pi\eta}$) in Equation 2 over the width of the resonance. Furthermore, the location of the $|S_{dn}|^2$ maximum does not coincide anymore with the energy at which the factor $(E_0 + \Delta - E)$ in Equation 3 is equal to zero, because of the energy dependence of the penetration factors over the width of the resonance. Therefore, there is no unique procedure for defining an energy, E_r, "at the center of the resonance" (Lane & Thomas 1958). In other words, for the exceptionally broad low-energy resonance in ^{3}H(d,n)^{4}He, we cannot chose the boundary condition parameter, $B_c = S_c(E_r)$, so that the level shift is zero at the location of the maximum of either $|S_{dn}|^2$, σ, or $S_{bare}(E)$, and at the same time expect the "center of the resonance", E_r, to equal the eigenvalue E_0 (see Section 3).[1]

[1] Jarmie et al. (1984) state that they "chose B_c so that the level shifts Δ_c are zero near the peak of the S function, which results in the level energy E_λ being close to the c.m. energy at which the S function peaks." Their Table VII lists the values of $a_d = 5.0$ fm, $a_n = 3.0$ fm and $B_d = -0.27864$, $B_n = -0.557$ for the channel radii and boundary conditions, respectively. However, the latter values correspond to an energy of $E_r = 90$ keV, which, contrary to their statement, is not near the peak of the astrophysical S factor (50 keV).

For example, consider again the blue curve shown in Figure 2, which was obtained with $E_0 = 0.0912$ MeV and $B_d = S_d(E_r) = -0.285$, where the latter value corresponds to an energy of $E_r = 0.0912$ MeV. If we chose instead to set the level shift equal to zero at the location of the $|S_{dn}|^2$ maximum (i.e., $E_r = 80$ keV), the eigenenergy needs to be chosen near 140 keV to achieve a good fit to the data, while keeping all other parameters constant. In other words, the eigenenergy is not located near the $|S_{dn}|^2$ maximum anymore. Conversely, if we set the eigenenergy equal to the location of the maximum of $|S_{dn}|^2$, σ, or $S_{bare}(E)$, good fits to the data require a level shift of zero near energies of $E_r = 0.092$ MeV, 0.096 MeV, and 0.098 MeV, respectively. We will explore the impact of boundary condition parameter variations on the fit results in Section 5.3.

5.2. *Results with fixed channel radii and boundary condition parameters*

We will first discuss the results of a Bayesian analysis where we keep the channel radii and boundary condition parameters at fixed values. We chose values of $a_d = 6.0$ fm, $a_n = 5.0$ fm and $B_d = -0.285$, $B_n = -0.197$, i.e., the same values as used in Barker (1997). The values for the boundary conditions correspond to a level shift of zero at an energy of $E_r = 0.0912$ MeV. We are interested to find out how our parameter estimates compare to previous results.

Our complete Bayesian model is specified in Appendix A. Here we will summarize only the key features. We consider five data sets (Section 2), consisting of 191 data points total. Experimental mean values for the measured energies and S-factors, together with estimates of statistical and systematic uncertainties, are given in Appendix B.

Our model includes 24 parameters: three R-matrix parameters (E_0, γ_d^2, and γ_n^2); electron screening potential (U_e); for each of the five data sets, intrinsic scatter for both energy and S-factor ($\sigma_{E,intr}$, $\sigma_{S,intr}$), systematic energy shift (f_E), and S-factor normalization (f_S). Normal likelihoods are used for the statistical and intrinsic uncertainties (see also Equations 13 and 15), because their magnitudes are relatively small.

The priors are obtained as follows. For the eigenenergy, E_0, we chose a weakly informative prior. Specifically, we adopt a normal density of zero mean value and 1.0 MeV standard deviation, which is restricted to positive energies only (i.e., a truncated normal density). Truncated normal densities are also assumed for the reduced widths (γ_d^2 and γ_n^2), with standard deviations given by the Wigner limits ($\gamma_{WL,d}^2$ and $\gamma_{WL,n}^2$) for the deuteron and neutron (Equation 8). For the electron

screening potential, we chose a truncated normal density with a standard deviation of 1.0 keV.

The systematic uncertainty of the measured energies is treated as a (positive or negative) offset (f_E). The original works report total energy uncertainties only, but do not provide specific information about the relative contributions of statistical and systematic effects. We will assume the prior, for each data set j, is given by a normal density with a mean value of zero and a standard deviation equal to the average reported total energy uncertainty in that experiment (Appendix B).

The systematic S-factor uncertainties for the data of Jarmie et al. (1984), Kobzev et al. (1966), Arnold et al. (1953), and Conner et al. (1952), discussed in Appendix B, amount to 1.26%, 2.5%, 2.0%, and 1.8%, respectively. These correspond to factor uncertainties of $(f.u.)_1 = 1.0126$, $(f.u.)_3 = 1.025$, $(f.u.)_4 = 1.020$, and $(f.u.)_5 = 1.018$, respectively. As explained in Section 4.3, we will use these values as shape parameters of lognormal priors for the systematic normalization factors, f_S, of each experiment. We already mentioned in Section 2 that Brown et al. (1987) did not determine absolute cross sections, but normalized their data to the results of Jarmie et al. (1984). We will include this data set in our analysis by choosing a weakly informative prior for the factor uncertainty, i.e., $(f.u.)_2 = 10$.

Finally, the intrinsic uncertainties for both energy and S-factor are inherently unknown to the experimenter. Thus we will assume very broad truncated normal priors, with standard deviations of 10 keV for the energy and 2 MeVb for the S-factor.

The MCMC sampling will provide the posteriors of all 24 parameters. We computed three MCMC chains, where each chain had a length of 100,000 steps after burn-in. The length of the burn-in was set to 50,000 steps for each chain. This ensured that the chains reached equilibrium and Monte Carlo fluctuations are negligible compared to the statistical, systematic, and intrinsic uncertainties.

The results for the S-factor are shown in Figure 3. The red lines represent 500 credible S-factor samples that were chosen at random from the total set of 100,000 samples. The marginalized posterior of the S-factor at a representative energy of 40 keV, near the center of the energy range important for fuison reactors and big bang nucleosynthesis, is shown in Figure 4. At this energy, we find a value of $S_{0.04}^{pres} = 25.46 \pm 0.20$ MeVb, where the uncertainties refer to 16, 50, and 84 percentiles. This value is also listed in Table 1. Our result can be compared to the previous value of $S_{0.04}^{prev} = 25.87 \pm 0.49$ MeVb from Bosch & Hale (1992), which was obtained using different methods and data selection. Present and previous values are in agreement, but our uncertainty is smaller by a factor of two.

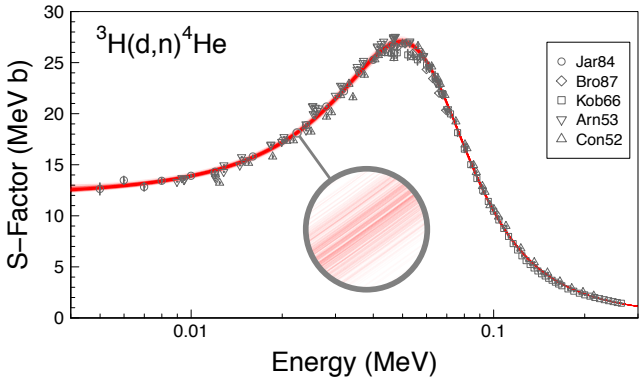

Figure 3. Astrophysical S-factors obtained from the Bayesian R-matrix fit. The data are the same as in Figure 1. The red lines represent credible S-factors computed using 500 sampled parameter sets that were chosen at random from the complete set of samples. The inset shows a magnified view of the S-factor samples.

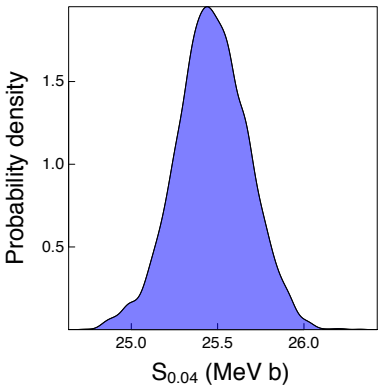

Figure 4. Marginalized posterior of the S-factor at a respresentative center-of-mass energy of 40 keV. Percentiles of the distribution are listed in Table 1.

Figure 5 presents the marginalized posterior densities of the eigenenergy (E_0), and the deuteron and neutron reduced widths (γ_d^2, γ_n^2). Numerical values of the R-matrix parameters are listed in Table 1. We find values of $E_0 = 0.0686^{+0.0051}_{-0.0040}$ MeV, $\gamma_d^2 = 1.42^{+0.44}_{-0.35}$ MeV, and $\gamma_n^2 = 0.0430^{+0.0097}_{-0.0077}$ MeV. These can be compared to the results of Barker (1997), also listed in Table 1, that were obtained using the same fixed values for the channel radii and boundary condition parameters. It can be seen that present and previous results differ significantly: our eigenvalue is lower by 23 keV, and our reduced withds are smaller by a factor of two. A more detailed comparison between present and previous results is difficult,

because no uncertainties have been presented in Barker (1997). In addition, somewhat different data sets have been analyzed in the two studies. For completion, we also list in Table 1 the values of the deuteron and neutron partial widths that are obtained from our results for the reduced widths according to Equation 4. We confirm previous findings (Conner et al. 1952; Argo et al. 1952) of the near equality of Γ_d and Γ_n, which causes the large low-energy cross section of the ^{3}H(d,n)^{4}He reaction (Section 1).

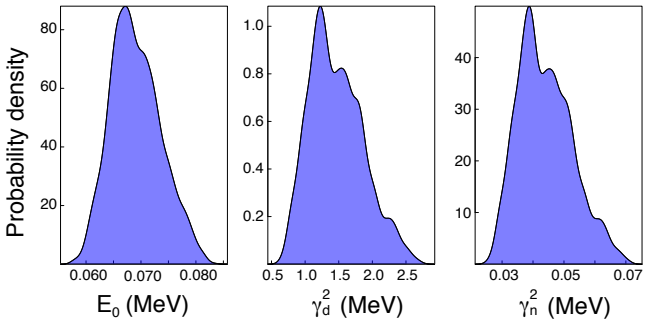

Figure 5. Marginalized posterior densities of the eigenenergy (E_0), and the deuteron and neutron reduced widths (γ_d^2, γ_n^2). Percentiles of the distributions are listed in Table 1.

Motivated by electron screening effects observed in ^{3}He(d,p)^{4}He S-factor data, Langanke & Rolfs (1989) investigated the data of Jarmie et al. (1984) and Brown et al. (1987) of the analog ^{3}H(d,n)^{4}He reaction. Based on a one-level R-matrix expression, Langanke & Rolfs (1989) report evidence of "electron screening effects caused by the electrons present in the target" at the lowest center-of-mass energies (≤ 16 keV). Since their R-matrix fit underpredicts the six lowest data points (see also Figure 3), they claim much better agreement if a screening potential of 41 eV (Thomas-Fermi model) or 27 eV (Hartree-Fock model) is included in the data fitting. Figure 6 shows our marginalized posterior density for the electron screening potential, U_e. It clearly demonstrates that there is no evidence of electron screening effects in the ^{3}H(d,n)^{4}He data, and only an upper limit can be extracted from the measurements. Integration of the posterior from zero to a percentile of 97.5% results in $U_e \leq 18.3$ eV (Table 1). We suspect that the erroneous claim of electron screening effects in the ^{3}H(d,n)^{4}He reaction by Langanke & Rolfs (1989) is most likely caused by the wrong sign of the level shift in the denominator of their one-level R-matrix expression (see their Equation 4).

Apart from the physical parameters (E_0, γ_d^2, γ_n^2, U_e), our Bayesian model also provides interesting information about systematic and intrinsic uncertainties of the data. The marginalized posteriors of the S-factor normalization factors, f_S, are displayed in Figure 7. Values for the percentiles of the distribution for each data set are listed in Table 2. The median values of f_S are equal to unity within $\approx 3\%$, indicating that reliable systematic uncertainty estimates were adopted for the data sets considered in the present analysis.

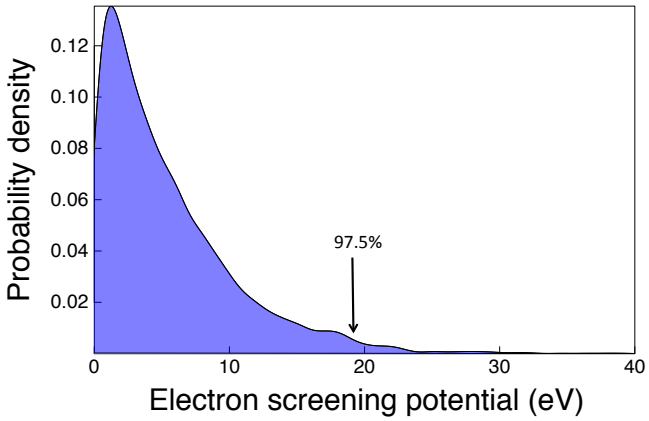

Figure 6. Marginalized posterior density for the electron screening potential, U_e. No evidence for electron screening in the ^{3}H(d,n)^{4}He reaction can be extracted from the available data, contrary to the claims of Langanke & Rolfs (1989), and only an upper limit for U_e can be obtained (Table 1).

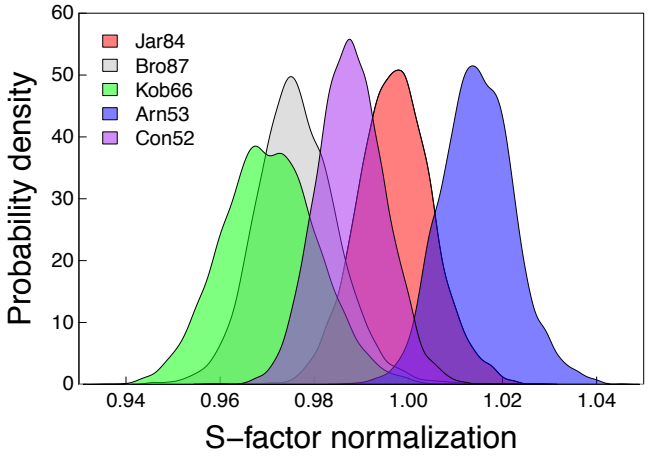

Figure 7. Marginalized posteriors of the S-factor normalization factors, f_S. The labels refer to the same data sets shown in Figure 1. Percentiles of the distributions are listed in Table 2.

Our values for the systematic energy shifts, f_E, for each data set are also listed in Table 2. Our results are consistent with the reported energy uncertainties, which are discussed in Appendix B. As expected, the largest systematic energy shifts are found for the data of Kobzev et al. (1966) ($f_{E,3} = 0.31^{+0.69}_{-0.75}$ keV) and Conner et al. (1952) ($f_{E,5} = 0.52 \pm 0.18$ keV).

The intrinsic uncertainties for energy and S-factor, $\sigma_{E,intr}$ and $\sigma_{S,intr}$, respectively, are almost all consistent with zero, and we provide in Table 2 upper limits based on 97.5 percentiles. The only exception is the intrinsic energy uncertainty for the data of Arnold et al. (1953), for which we find a value of $\sigma_{E,intr,4} = 1.33^{+0.26}_{-0.39}$ keV. Although this indicates that the energy uncertainties have been underestimated in Arnold et al. (1953) (see also discussion in Appendix B), the effect is naturally accounted for in our Bayesian analysis.

5.3. *Results including the sampling of the channel radii and boundary condition parameters*

The results discussed so far were obtained assuming fixed values for the channel radii and boundary condition parameters (Section 5.2). However, as explained in Section 3, there is considerable freedom in the choice of these parameters, which, therefore, should be included in the sampling.

Descouvemont & Baye (2010) recommended to chose the channel radius so that its value exceeds the sum of the radii of the colliding nuclei. In a given reaction, the radii of the different channels do usually not have the same value. Previous studies either adopted *ad hoc* values, or derived the channel radii from data. Argo et al. (1952) and Hale, Brown & Paris (2014) assumed equal neutron and deuteron channel radii, and find best-fit values of 7.0 fm from analyzing ^{3}H(d,n)^{4}He data. Woods et al. (1988) measured the ^{4}He(^{7}Li,^{6}Li)^{5}He and ^{4}He(^{7}Li,^{6}He)^{5}Li stripping reactions and found a value of $a_n = 5.5 \pm 1.0$ fm from fitting the experimental line shapes. Jarmie et al. (1984) and Brown et al. (1987) assumed radii of $a_d = 5.0$ fm and $a_n = 3.0$ fm. The latter value presumably originated from Adair (1952) and Dodder & Gammel (1952), who adopted $a_n = 2.9$ fm to fit the low-energy ^{4}He + *nucleon* phase shifts. In the present work, we will chose uniform priors between 2.5 fm and 10.0 fm,

$$a_d \sim U(2.5, 10.0) \ , \quad a_n \sim U(2.5, 10.0) \qquad (22)$$

The boundary condition parameter of a given channel is most frequently chosen in the literature so that the eigenvalue, E_0, is equal to the energy, E_r, at which the level shift is zero, i.e., $B_c = S_c(E_r)$ (Section 3; see, e.g., Barker (1997)). In Section 5.1, we discussed the complications that arise when choosing the arbitrary value of the boundary condition parameter in the case of a broad resonance. Lane & Thomas (1958) recommended to chose B_c in the one-level approximation so that the eigenvalue E_0 lies within the width of the observed resonance. Therefore, we will chose for E_0 a uniform prior between 20 keV and 80 keV (see Figure 3). For the energy E_r, at which the level shift is zero, we use a uniform prior between zero and 1.0 MeV. In summary,

$$E_0 \sim U(0.02, 0.08) \ , \quad E_r \sim U(0.0, 1.0) \qquad (23)$$

Our Bayesian model contains now 11 parameters.

We computed 10 individual MCMC chains to test the stability of the fitting procedure, where each chain had a length of 100,000 steps (after burn-in). All 10 chains gave S-factor results that were again close to those shown in Figure 3. Considering all 10 MCMC chains together, we find at 40 keV a value of 25.93±0.30 MeVb for the S-factor. This value, which is listed in Table 2, agrees with the result of the eight-parameter fit discussed in Section 5.2. Therefore, including the channel radii and boundary condition parameters in the sampling has no noticeable effect on the derived S-factor of the ^{3}H(d,n)^{4}He reaction.

Table 2 also lists numerical results for the normalization factors of the four data sets (f_1, f_2, f_3, f_4) and the intrinsic uncertainty (σ_{intr}). Their values are consistent with the results of the eight-parameter fits (Table 1) and, therefore, are not significantly affected by varying the channel radii or boundary condition parameters.

We will now discuss the results for the resonance parameters. As can be seen from Table 2, the eigenenergy, E_0, has a large uncertainty (±20 keV), indicating that its posterior extends over the entire range of its prior (Equation 23). This is expected, since variations in E_0 over the width of the observed resonance can be easily compensated by adjusting the value of E_r, as discussed in Section 5.1. For E_r, we find a value of $0.0753^{+0.0046}_{-0.0030}$ MeV. Since both our eight-parameter fit (Table 1) and Barker (1997) assumed $E_0 = E_r$, the values of these energies cannot be directly compared with the numerical results for the eleven-parameter fit listed in Table 2.

Across the ten computed MCMC chains, the shapes of the posterior for both channel radii, a_d and a_n, vary significantly, and frequently double- or triple-peaked structures are obtained. Taken all chains together, we obtain values of $a_d = 2.77^{+0.60}_{-0.21}$ fm and $a_n = 6.5^{+2.3}_{-2.6}$ fm. Our result for the neutron channel radius has a large uncertainty and agrees with previously obtained best-fit values of Argo et al. (1952), Hale, Brown & Paris (2014), and Woods et al. (1988), but disagrees with the early works of Adair (1952) and Dodder & Gammel (1952) (Table 2). Furthermore, our estimate for the deuteron channel radius is significantly smaller compared to the results of Argo et al. (1952), Hale, Brown & Paris (2014), and Woods et al. (1988). Notice, however, that their values were not fit independently since they arbitrarily assumed $a_d = a_n$.

Finally, we discuss the results for the widths. We will not report values for the reduced widths, γ_d^2 and γ_n^2, which depend strongly on a_d and a_n, respectively, since the channel radii were fit parameters. Instead, we will report values for the partial widths, Γ_d and Γ_n. For the latter quantities, an increase of the channel radius, a_c, causes a reduction in the reduced width, $\gamma_{\lambda c}^2$, but at the same time an increase in the penetration factor, P_c (see Equations 4 and 9). Taken all ten chains together, we obtain best-fit values of $\Gamma_d = 0.14^{+0.30}_{-0.10}$ MeV and $\Gamma_n = 0.54^{+0.90}_{-0.21}$ MeV (Table 2). Therefore, we find $\Gamma_d \approx \Gamma_n$ within uncertainties, which explains the large cross section of the ^{3}H(d,n)^{4}He reaction at low energies, as explained in Section 1. Our value of Γ_n agrees with the result of Barker (1997), but we find a smaller value of Γ_d. The difference is most likely caused by the different deuteron channel radii derived here compared to the value assumed in the previous work (Table 2).

6. THERMONUCLEAR REACTION RATES

The thermonuclear reaction rate per particle pair, $N_A\langle\sigma v\rangle$, at a given plasma temperature, T, can be written as (Iliadis 2015)

$$N_A\langle\sigma v\rangle = \left(\frac{8}{\pi m_{01}}\right)^{1/2} \frac{N_A}{(kT)^{3/2}} \int_0^\infty e^{-2\pi\eta}\, S(E)\, e^{-E/kT}\, dE \quad (24)$$

where m_{01} is the reduced mass of projectile and target, N_A is Avogadro's constant, and k is the Boltzmann constant. Thermonuclear reaction rates are calculated by numerical integration of Equation 24. The S-factor is calculated from the samples of the eleven-parameter Bayesian R-matrix fit, discussed in Section 5.3, and thus our new rates contain the effects of varying channel radii and boundary condition parameters. Our rate is based on 5,000 random MCMC samples, which ensures that Monte Carlo fluctuations are negligible compared to the rate uncertainties. Our lower integration limit was 1 eV, and rates are computed for 46 different temperatures between 1 MK and 1 GK. Recommended rates are computed as the 50th percentile of the probability density, while the rate factor uncertainty, f.u., is obtained from the 16th and 84th percentiles (Longland et al. 2010). Numerical reaction rate values are listed in Table 3. At the highest temperatures, $T = 1.25 - 10$ GK, higher-lying resonances impact the rates and, therefore, we adopted in this range the results of Descouvemont et al. (2004).

Reaction rates are displayed in Figure 8. Our low (16th percentile), median, and high (84th percentile) rates, divided by the present median rates, are shown as a gray band. The rate uncertainties in the temperature region between 1 MK and 1 GK are between 1.1% and 1.5%. While a number of previous works have presented ^{3}H(d,n)^{4}He thermonuclear rates or, equivalently, thermal reactivities (see, e.g., Bosch & Hale (1992)), most do not present uncertainties and, therefore, a direct comparison to our results is not very meaningful. The only recently published ^{3}H(d,n)^{4}He rates with uncertainties can be found in Descouvemont et al. (2004). Their "lower", "adopted", and "upper" rates, divided by our median rate, are shown as the purple band in Figure 8. Compared to the present rates, the previous results are higher by up to 2.5% at temperatures below 0.018 GK, and lower by up to 2.5% at higher temperatures. Interestingly, the previous rate uncertainties, estimated using traditional statistical methods (i.e., χ^2 fitting), are much smaller compared to our results. For example, at the temperature where big bang nucleosynthesis ensues (1 GK), the R-matrix analysis of Descouvemont et al. (2004) predicts a rate uncertainty of only 0.6%, compared to 1.4% in the present work (Table 3). The difference is likely caused by using fixed values for the channel radii and boundary condition parameters and by combining systematic and statistical uncertainties during the fit in the previous work, while all relevant parameters, including channel radii, boundary condition parameters, and data set normalization factors were sampled in the present Bayesian analysis (Section 5.3).

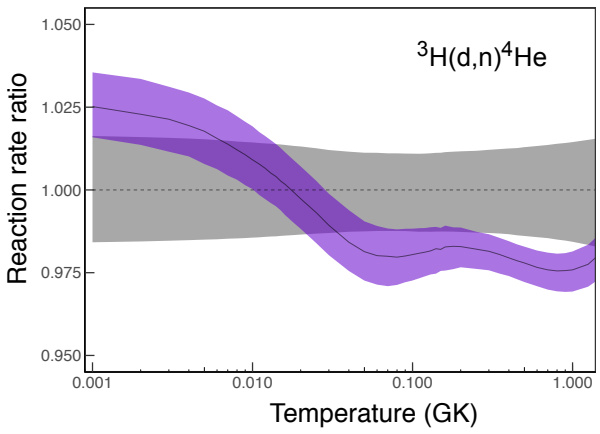

Figure 8. Present ^{3}H(d,n)^{4}He thermonuclear rates compared to a recent evaluation (Descouvemont et al. 2004). The gray shaded area corresponds to our new Bayesian rate, while the purple shaded area depicts the previous rates. The bands signify a 68% coverage probability. All rates are normalized to the new recommended rate. The solid line shows the ratio of previous and present recommended rates.

7. SUMMARY AND CONCLUSIONS

This work presented the first Bayesian R-matrix analysis of ^{3}H(d,n)^{4}He S-factors and thermonuclear reaction rates. We evaluated the published data and adopted only those sets for which separate estimates of systematic and statistical uncertainties can be obtained. The difficulties and special circumstances when studying the low-energy resonance in this reaction are discussed in detail. We analyzed the low-energy S-factor data using a two-channel, single-level R-matrix approximation that is implemented in a Bayesian model. Thermonuclear reaction rates are found by numerically integrating the Bayesian S-factor samples. Our resulting rate uncertainties are between 1.1% and 1.5%. At the relevant temperatures, our new rates differ by up to 2.5% compared to previous estimates. Our rate uncertainties are larger, but more reliable, than previous results, since unlike previous studies we sampled all relevant model parameters, including channel radii, boundary condition parameters, and data set normalization factors. The present study demonstrates the usefulness of the Bayesian approach for estimating R-matrix parameters, S-factors, and reaction rates. The results will prove useful in future studies that involve multiple channels and resonances. Finally, unlike previous claims, we find no evidence for the electron screening effect in any of the published ^{3}H(d,n)^{4}He reaction data.

We would like to thank Caleb Marshall for helpful comments. This work was supported in part by NASA under the Astrophysics Theory Program grant 14-ATP14-0007, and the U.S. DOE under contracts DE-FG02-97ER41041 (UNC) and DE-FG02-97ER41033 (TUNL).

Software: JAGS

APPENDIX

A. BAYESIAN MODEL LIKELIHOODS AND PRIORS

Information regarding our Bayesian model is provided below. For the sampling with fixed values of channel radii and boundary condition parameters, the likelihoods and priors are given in symbolic notation as:

Parameters:

$$\theta \equiv (E_0, \gamma_d^2, \gamma_n^2, U_e, \sigma_{E,intr,j}, \sigma_{S,intr,j}, f_{E,j}, f_{S,j}) \tag{A1}$$

Likelihoods for energy:

$$E_i' \sim N(E_i, \sigma_{E,intr,j}^2) \tag{A2}$$

$$E_{i,j}'' = f_{E,j} + E_i' \tag{A3}$$

$$E_{i,j}^{exp} \sim N(E_{i,j}'', \sigma_{E,stat,i}^2) \tag{A4}$$

Likelihoods for S-factor:

$$S_i' \sim N(S_i, \sigma_{S,intr,j}^2) \tag{A5}$$

$$S_{i,j}'' = f_{S,j} \times S_i' \tag{A6}$$

$$S_{i,j}^{exp} \sim N(S_{i,j}'', \sigma_{S,stat,i}^2) \tag{A7}$$

Priors:

$$E_0 \sim N(0.0, 1.0^2)T(0,) \tag{A8}$$

$$(\gamma_d^2, \gamma_n^2) \sim N(0.0, (\gamma_{WL}^2)^2)T(0,) \tag{A9}$$

$$U_e \sim N(0.0, 0.001^2)T(0,) \tag{A10}$$

$$E_i \sim U(0.001, 0.3) \tag{A11}$$

$$\sigma_{E,intr,j} \sim N(0.0, 0.01^2)T(0,) \tag{A12}$$

$$f_{E,j} \sim N(0.0, \xi_j^2) \tag{A13}$$

$$\sigma_{S,intr,j} \sim N(0.0, 2.0^2)T(0,) \tag{A14}$$

$$f_{S,j} \sim LN(0, [\ln(f.u.)_j]^2) \tag{A15}$$

where the indices $j = 1, ..., 5$ and $i = 1, ..., 191$ label the data set and the data points, respectively. The symbols have the following meaning: level eigenvalue (E_0), reduced deuteron and neutron widths (γ_d^2, γ_n^2), electron screening

potential (U_e), intrinsic uncertainty for energy ($\sigma_{E,intr}$) and S-factor ($\sigma_{S,intr}$), systematic energy offset (f_E) and S-factor normalization (f_S), experimental systematic factor uncertainty of S-factor ($f.u.$), Wigner limit (γ^2_{WL}), measured energy (E^{exp}) and measured S-factor (S^{exp}); true energy (E); the true S-factor (S) is calculated from the R-matrix expression (Equations 1 − 3) using the R-matrix parameters (E_0, γ^2_d, γ^2_n); N, U, and LN denote normal, uniform, and lognormal probability densities, respectively; $T(0,)$ indicates that the distribution is only defined for positive random variables; "∼" stands for "sampled from." All numerical values of energy and S-factor variables are in units of MeV and MeVb, respectively. For the standard deviation, ξ_j, of the prior for the systematic energy offset, $f_{E,j}$, we adopted the average value for the reported energy uncertainties of a given experiment, j (see Appendix B). For more information on the choice for the numerical values of the priors, see the text.

B. NUCLEAR CROSS SECTION DATA FOR ^{3}H + d → n + ^{4}He

We discuss here the current status of the available data for the ^{3}H(d,n)^{4}He reaction. Several works have measured only differential cross sections at a single angle, and assumed an isotropic angular distribution to derive the total cross section. Figure 4 in Conner et al. (1952) shows that the integrated cross section data points agree with the theoretical single-level dispersion curve (solid line) at deuteron bombarding energies of ≤ 450 keV. Therefore, at these low energies, the cross section is determined by the $3/2^+$ (s-wave) resonance in ^{3}H + d (see Section 1), and the angular distribution can be assumed to be nearly isotropic; see also Bém et al. (1997). At higher energies, higher-lying levels in ^{5}He will impact the cross section, giving rise to anisotropies in the differential cross section. In the present work, we only take data in this low-energy range into account (corresponding to bombarding triton energies of ≤ 680 keV, or center-of-mass energies of ≤ 270 keV), which is of primary interest for ^{3}H + d thermonuclear fusion. As noted in Section 5.2, we will adopt in our analysis only those data sets for which we can separately estimate statistical and systematic uncertainties.

B.1. *The ^{2}H(t,α)n Data of Jarmie et al. (1984)*

The measurement of Jarmie et al. (1984) was performed using a triton beam incident on a windowless deuterium gas target. This technique minimizes systematic beam energy uncertainties compared to other measurements that used a gas target contained by foils. Our adopted center-of-mass energies and astrophysical S-factors are listed in Table 4. The energies (E_{cm} = 5 − 47 keV) correspond to the center of the gas target and were calculated from the laboratory energies listed in column 2 of Table V in Jarmie et al. (1984). The total (systematic plus statistical) uncertainties of the center-of-mass energies are less than 6 eV. The S-factors are taken from column 3 of their Table VI. Their statistical uncertainties amount to 0.5% − 4.6%, depending on energy (see their Table III). The systematic uncertainty is 1.26% (see their Table IV).

B.2. *The ^{3}H(d,α)n Data of Brown et al. (1987)*

The ^{3}H(d,α)n measurement of Brown et al. (1987) was performed with an apparatus similar to the one described in Jarmie et al. (1984), except that a deuteron beam (E_d = 80 − 116 keV) was incident on a triton gas target. However, no absolute normalization was determined in Brown et al. (1987). For the purpose of reporting their data, Brown et al. (1987) determined an approximate scale by matching the cross sections in the overlapping energy region to the earlier absolute measurement of Jarmie et al. (1984). The reported astrophysical S-factors versus center-of-mass energies are listed in Table 5. Since they represent relative results only, we implemented these data into our analysis using a weakly informative prior for the normalization factor (Section 4). The statistical uncertainties amount to 0.8%.

B.3. *The ^{2}H(t,α)n Data of Kobzev et al. (1966)*

Kobzev et al. (1966) measured the ^{2}H(t,α)n cross section at 90° in the triton bombarding energy range of E_t = 115 − 1650 keV. They employed mica foils of 0.16 mg/cm^2 and 0.31 mg/cm^2 thickness as entrance windows of their deuterium gas target. Below a triton bombarding energy of ≈ 660 keV, the differential cross section is isotropic (Conner et al. 1952; Argo et al. 1952) and, therefore, we calculated the total cross section by multiplying the values listed in their table by a factor of 4π. Our adopted S-factors are given in Table 6. Regarding the uncertainties in the bombarding energy, Kobzev et al. (1966) state "The interaction energy of tritium and deuterium nuclei was determined with 2.5% accuracy in the range 115 − 150 keV, with 2% accuracy in the range 150 − 1200 keV....." We adopted these uncertainties (see Table 6) and assume that they refer to statistical effects. Furthermore, they state "The differential cross section was measured from 115 to 400 keV with 2% accuracy[,] in the range 400 − 800 keV with 2.5% accuracy..."

Although Kobzev et al. (1966) do not provide separate estimates of statistical and systematic uncertainties, we will assume that the quoted values are of statistical nature. For the systematic uncertainty in their measurement, we assume a value of 2.5%.

B.4. *The ^{3}H(d,n)^{4}He Data of Arnold et al. (1953)*

Arnold et al. (1953) measured cross sections of the ^{3}H(d,n)^{4}He reaction between 10 keV and 120 keV deuteron bombarding energy, using thin ($5 - 10$ μg/cm^2) SiO entrance foils for their tritium gas target. Their results were later published in Arnold et al. (1954), and Table III in the latter paper served as the main source for their cross sections in most previous analyses; see, e.g., Angulo et al. (1999). However, Arnold et al. (1954) did not report the originally measured cross sections of Arnold et al. (1953) in their Table III. What is listed there are energies and cross sections derived from a "smoothed curve" based on the energy dependence of the Gamow factor, and these values should not be used in fitting the data. The original data are provided in Table VI of Arnold et al. (1953), which we adopted in our analysis.

We disregarded the data points at the lowest deuteron bombarding energies of $7 - 11$ keV "...because failure of the counter collimating system and excess production of condensable vapor gave good reason to expect that the experimental value of the cross sections at these energies might be low." Furthermore, the listed cross section values at $E_d = 24.96$ keV, 24.91 keV, and 24.89 keV are certainly affected by a decimal-point error, since they are too large by one order of magnitude. Similarly, the listed cross section values at $E_d = 49.62$ keV and 49.60 keV are too low by one order of magnitude. Therefore, we disregarded these five data points.

Arnold et al. (1953) provide a detailed list of uncertainties in their Table VIII. Statistical uncertainties amount to 0.2% and 0.1% at deuteron bombarding energies below and above ≈ 40 keV, respectively. Our derived center-of-mass energies and S-factors are listed in Table 7. Arnold et al. (1953) quoted systematic S-factor uncertainties ("standard error") of 1.8%, 1.5%, and 1.4% at deuteron bombarding energies of 25 keV, 50 keV, and 100 keV, respectively. In the present work, we adopted a constant systematic S-factor uncertainty of 2.0%. The uncertainty in the center-of-mass energy is not directly stated in Arnold et al. (1953), but can be estimated based on the information provided. They write "...at 10 keV, 100 V of change cause a 6 percent change in cross section..." From their Table II, considering only the S-factor uncertainties listed under "5. Energy," we estimate an uncertainty of about ± 75 eV for the center-of-mass energy. We will adopt this value for all of their measured energies.

B.5. *The ^{3}H(d,n)^{4}He Data of Conner et al. (1952)*

The cross section data of Conner et al. (1952) were obtained in two experiments, using different ion accelerators, for deuteron bombarding energies between 10 keV and 1732 keV. We adopted the differential cross sections measured at 90° from their Tables I and II. We assumed an isotropic angular distribution at low energies and multiplied their differential cross section by 4π to find the total reaction cross section. Our adopted S-factors are given in Table 8. Conner et al. (1952) state that the "statistical probable error of the values from each target was about 1 percent except for the points at 10.3 and 15.4 keV." We disregarded these lowest energy data points because no other information is provided regarding their cross section uncertainty. For the systematic S-factor uncertainty, based on the effects of the finite solid angle, number of target atoms, and number of incident beam particles, they quote a combined uncertainty of 1.8%. The uncertainty in the center-of-mass energy is not directly stated in Conner et al. (1952), but can be estimated based on the number of significant figures shown in their Tables I and II. We estimate an energy uncertainty of ± 60 eV at 12.4 keV and ± 600 eV at 214 keV center-of-mass energy.

B.6. *Other Data*

The following data sets were excluded from our analysis. The data of Bretscher & French (1949) are much smaller in magnitude compared to other data, and do not show the maximum of the resonance. The S-factor data of Jarvis & Roaf (1953) display an energy dependence that contradicts all other measurements; see, for example, Figure 2 in Bosch & Hale (1992). The ^{2}H(t,n)^{4}He measurement of Argo et al. (1952) employed relatively thick (1.5 mg/cm^2) aluminum entrance foils for their deuterium gas target. For example, tritons of 183 keV laboratory energy, after passing the entrance foil, would have lost an energy of 568 keV in the foil, giving rise to a beam straggling of $\approx$ 31 keV. Consequently, the uncertainties of the effective beam energy will be significant. Argo et al. (1952) stated that the beam energy *loss* was determined "to within ± 5 keV," but not enough information was provided regarding the total uncertainty of the effective beam energy. Also, Argo et al. (1952) stated that their cross section data "...have an

estimated over-all accuracy of ±10%; this ±10 percent arises almost entirely from the straggling and energy correction uncertainties up to energies of about 300 keV..." However, insufficient information is provided to disentangle the contributions of statistical and systematic effects to the total uncertainty.

REFERENCES

Adair, R.K. 1952, Phys. Rev. 86, 155

Angulo, C., et al. 1999, Nucl. Phys. A 656, 3

Argo, H.V., Taschek, R.F., Agnew, H.M., Hemmedinger, A., & Leland, W.T. 1952, Phys. Rev. 87, 612

Arnold, W.R., Phillips, J.A., Sawyer, G.A., Stovall, Jr., E.J., & Tuck, J.L. 1953, Absolute Cross Section for the Reaction T(d,n)^{4}He from 10 to 120 keV, Tech. Rep. LA-1479, Los Alamos Scientific Laboratory, Los Alamos, NM

Arnold, W.R., Phillips, J.A., Sawyer, G.A., Stovall, Jr., E.J., & Tuck, J.L. 1954, Phys. Rev. 93, 483

Bame Jr., S.J., & Perry Jr., J.E. 1957, Phys. Rev. 107, 1616

Assenbaum, H.J., Langanke, K., & Rolfs, C. 1987, Z. Phys. A 327, 461

Barit, I.Y., & Sergeev, V.A. 1971, in: Nuclear Physics and Interaction of Particles with Matter, ed. D.V. Skobel'tsyn (Springer Science, New York)

Barker, F.C. 1997, Phys. Rev. C 56, 2646

Barker, F.C., & Woods, C.L. 1985, Austr. J. Phys. 38, 563

Bém, P., Kroha, V., Mares, J., Simecková, E., Trginová, & Vercimák, P. 1997, Few-Nucleon Sys. 22, 77

Bosch, H.S., & Hale, G.M. 1992, Nucl. Fusion 32, 611-632; Erratum: 1993, Nucl. Fusion 33, 1919

Bretscher, E., & French, A.P. 1949, Phys. Rev. 75, 1154

Brown, R.E., Jarmie, N., & Hale, G.E. 1987, Phys. Rev. C 35, 1999-2004

Brown, L.S., & Hale, G.M. 2014, Phys. Rev. C, 89, 014622

Coc, A., Petitjean, P., Uzan, J.-Ph., Vangioni, E., Descouvemont, P., Iliadis, C., & Longland, R. 2015, Phys. Rev. D 92, 123526

Conner, J.P., Bonner, T.W., & Smith, J.R. 1952, Phys. Rev. 88, 468-473

Descouvemont, P., Adahchour, A., Angulo, C., Coc, A., & Vangioni-Flam, E. 2004, At. Data Nucl. Data Tabl. 88, 203

Descouvemont, P., & Baye, D. 2010, Rep. Prog. Phys. 73, 036301

de Souza, R.S., Iliadis, C., & Coc, A. 2018, ApJ, submitted

Dodder, D.C., & Gammel, J.L. 1952, Phys. Rev. 88, 520

Dover, C.B., Mahaux, C., & Weidenmüller, H.A. 1969, Nucl. Phys. A 139, 593

Duane, B.H. 1972, Rep. BNWL-1685, Battelle Pacific Northwest Laboratory, Richland, WA

Engstler, S., Krauss, A., Neldner, K., Rolfs, C., Schröder, U., & Langanke, K. 1988, Phys. Lett. B 202, 179

Geyer, C. J. 2011, in *Handbook of Markov Chain Monte Carlo* (Chapman and Hall/CRC)

Gómez Iñesta, Á, Iliadis, C., & Coc, A. 2017, ApJ, 849, 134

Hale, G.M., Brown, R.E., & Jarmie, N. 1987, Phys. Rev. Lett. 59, 763

Hale, G.M., Brown, L.S., & Paris, M.W. 2014, Phys. Rev. C 89, 014623

Hastings, W. K. 1970, Biometrika, 57, 97

Heinrich, J., & Lyons, L. 2007, Annu. Rev. Nucl. Part. Sci., 57, 145

Hilbe, J.M., de Souza, R.S., & Ishida, E.E.O. 2017, Bayesian Models for Astrophysical Data Using R, JAGS, Python, and Stan (Cambridge University Press)

Iliadis, C. 2015, *Nuclear Physics of Stars*, (2nd Edition; Weinheim; Wiley-VCH)

Iliadis, C., Anderson, K.S., Coc, A., Timmes, F.X., & Starrfield, S. 2016, ApJ, 831, 107

Jarmie, N., Brown, R.E., & Hardekopf, R.A. 1984, Phys. Rev. C 29, 2031-2046; 1984, Erratum: Phys. Rev. C 33, 385

Jarvis, R.G., & Roaf, D. 1953, Proc. R. Soc. Lond. A 218, 432-438

Jaynes, E., & Bretthorst, G. 2003, Probability Theory: The Logic of Science (Cambridge University Press)

Kim, Y., et al. 2012, Phys. Rev. C 85, 061601(R)

Kobzev, A.P., Salatskij, V.I., & Telezhnikov, S.A. 1966, Sov. J. Nucl. Phys. 3, 774-776

Lane, A.M., & Thomas, R.G. 1958, Rev. Mod. Phys. 30, 257

Langanke, K., & Rolfs, C. 1989, Mod. Phys. Lett. A 4, 2101

Longland, R., Iliadis, C., Champagne, A. E., Newton, J. R., Ugalde, C., Coc, A., & Fitzgerald, R. 2010, Nucl. Phys. A, 841, 1

Metropolis, N., Rosenbluth, A. W., Rosenbluth, M. N., Teller, A. H., and Teller, E. 1953, J. Chem Phys., 21, 1087

Peres, A.J. 1979, J. Nucl. Mater. 50, 5569

Plummer, M. 2003, *JAGS: A program for analysis of Bayesian graphical models using Gibbs sampling*, in: Proceedings of the 3rd International Workshop on Distributed Statistical Computing (dsc 2003), Vienna, Austria, ISSN 1609-395X

R Core Team 2015, *R: A language and environment for statistical computing*, R Foundation for Statistical Computing, Vienna, Austria (https://www.R-project.org/)

Teichmann, T., & Wigner, E.P. 1952, Phys. Rev. 87, 123

Tilley, D.R., Cheves, C.M., Godwin, J.L., Hale, G.M., Hofmann, H.M., Kelley, J.H., Sheu, C.G., & Weller, H.R. 2002, Nucl. Phys. A 708, 3

Wilson, D.C., et al. 2008, Rev. Sci. Instr. 79, 10E525 (2008)

Woods, C.L., Barker, F.C., Catford, W.N., Fifield, L.K., and Orr, N.A. 1988, Aust. J. Phys. 41, 525

Table 1. Results of Bayesian fits (I)[a].

Parameter	Present[b]	Previous
E_0 (MeV)	$0.0686^{+0.0051}_{-0.0040}$	0.0912[d]
γ_d^2 (MeV)	$1.42^{+0.44}_{-0.35}$	2.93[d]
γ_n^2 (MeV)	$0.0430^{+0.0097}_{-0.0077}$	0.0794[d]
Γ_d (MeV)	$0.26^{+0.12g}_{-0.08}$	0.645[d]
Γ_n (MeV)	$0.294^{+0.067g}_{-0.053}$	0.543[d]
U_e (eV)	≤ 18.3	41 or 27[e]
$S_{0.04}$ (MeVb)[c]	25.46±0.20	25.87±0.49[f]

[a] More results are listed in Table 2. The values of the channel radii and boundary condition parameters were fixed at $a_d = 6.0$ fm, $a_n = 5.0$ fm, $B_d = -0.285$, and $B_n = -0.197$, i.e., the same values as used in Barker (1997); the values of B_c correspond to an energy of $E_r = 0.0912$ MeV.

[b] Uncertainties represent 16th, 50th, and 84th percentiles, while upper limits correspond to 97.5% credibility.

[c] S-factor at 40 keV.

[d] From Barker (1997); no uncertainty estimates were provided.

[e] From Langanke & Rolfs (1989); the first and second value is obtained from the Thomas-Fermi model and the Hartree-Fock model, respectively.

[f] From Table V of Bosch & Hale (1992); the uncertainty is given in their Table IV.

[g] Calculated from the values of the reduced widths, γ_d^2 and γ_n^2, listed in the rows above.

Table 2. Results of Bayesian fits (II).[a]

Parameter[b]	Value[d]	xxx
$\sigma_{E,intr,1}$ (keV)	$\leq$0.65	
$\sigma_{E,intr,2}$ (keV)	$\leq$2.3	
$\sigma_{E,intr,3}$ (keV)	$\leq$1.2	
$\sigma_{E,intr,4}$ (keV)	$1.33^{+0.26}_{-0.39}$	
$\sigma_{E,intr,5}$ (keV)	$\leq$2.0	
$\sigma_{S,intr,1}$ (MeVb)	$\leq$0.20	
$\sigma_{S,intr,2}$ (MeVb)	$\leq$0.68	
$\sigma_{S,intr,3}$ (MeVb)	$\leq$0.084	
$\sigma_{S,intr,4}$ (MeVb)	$\leq$0.48	
$\sigma_{S,intr,5}$ (MeVb)	$\leq$0.52	
$f_{E,1}$ (keV)	-0.0002 ± 0.0060	
$f_{E,2}$ (keV)	-0.0001 ± 0.0088	
$f_{E,3}$ (keV)	$0.31^{+0.69}_{-0.75}$	
$f_{E,4}$ (keV)	-0.049 ± 0.074	
$f_{E,5}$ (keV)	0.52 ± 0.18	
$f_{S,1}$	0.9971 ± 0.0076	
$f_{S,2}$	$0.9759^{+0.0085}_{-0.0078}$	
$f_{S,3}$	0.970 ± 0.010	
$f_{S,4}$	1.0146 ± 0.0074	
$f_{S,5}$	0.9877 ± 0.0071	

[a] Results listed here complement those listed in Table 1. The values of the channel radii and boundary condition parameters were fixed at $a_d = 6.0$ fm, $a_n = 5.0$ fm, $B_d = -0.285$, and $B_n = -0.197$, i.e., the same values as used in Barker (1997); the values of B_c correspond to an energy of $E_r = 0.0912$ MeV.

[b] The symbols $\sigma_{E,intr}$, $\sigma_{S,intr}$, f_E, and f_S denote the intrinsic uncertainty in energy and S-factor, the systematic energy shift, and the S-factor normalization, respectively; the indices, $j = 1...5$, label the five different data sets: (1) Jarmie et al. (1984); (2) Brown et al. (1987); (3) Kobzev et al. (1966); (4) Arnold et al. (1953); (5) Conner et al. (1952).

[c] Uncertainties represent 16th, 50th, and 84th percentiles, while upper limits correspond to 97.5% credibility.

Table 3. Recommended ^{3}H(d,n)^{4}He Reaction Rates[a].

T (GK)	Median	f.u.	T (GK)	Median	f.u.
0.001	1.938E-07	1.015	0.140	1.061E+08	1.011
0.002	1.405E-03	1.015	0.150	1.229E+08	1.011
0.003	1.020E-01	1.014	0.160	1.400E+08	1.011
0.004	1.502E+00	1.014	0.180	1.744E+08	1.011
0.005	1.011E+01	1.014	0.200	2.081E+08	1.011
0.006	4.314E+01	1.014	0.250	2.852E+08	1.011
0.007	1.370E+02	1.014	0.300	3.488E+08	1.012
0.008	3.550E+02	1.014	0.350	3.988E+08	1.012
0.009	7.927E+02	1.014	0.400	4.371E+08	1.012
0.010	1.582E+03	1.014	0.450	4.655E+08	1.012
0.011	2.893E+03	1.014	0.500	4.862E+08	1.012
0.012	4.934E+03	1.014	0.600	5.105E+08	1.012
0.013	7.951E+03	1.013	0.700	5.194E+08	1.013
0.014	1.222E+04	1.013	0.800	5.190E+08	1.013
0.015	1.807E+04	1.013	0.900	5.129E+08	1.013
0.016	2.583E+04	1.013	1.000	5.034E+08	1.014
0.018	4.859E+04	1.013	1.250	*4.624E+08*	*1.007*
0.020	8.377E+04	1.013	1.500	*4.325E+08*	*1.007*
0.025	2.498E+05	1.012	1.750	*4.044E+08*	*1.007*
0.030	5.761E+05	1.012	2.000	*3.792E+08*	*1.008*
0.040	1.958E+06	1.012	2.500	*3.369E+08*	*1.008*
0.050	4.695E+06	1.011	3.000	*3.039E+08*	*1.009*
0.060	9.141E+06	1.011	3.500	*2.776E+08*	*1.009*
0.070	1.550E+07	1.011	4.000	*2.564E+08*	*1.010*
0.080	2.384E+07	1.011	5.000	*2.244E+08*	*1.010*
0.090	3.407E+07	1.011	6.000	*2.017E+08*	*1.011*
0.100	4.602E+07	1.011	7.000	*1.847E+08*	*1.011*
0.110	5.945E+07	1.011	8.000	*1.716E+08*	*1.012*
0.120	7.412E+07	1.011	9.000	*1.612E+08*	*1.012*
0.130	8.976E+07	1.011	10.00	*1.527E+08*	*1.013*

[a]Reaction rates in units of cm^{3} mol^{-1} s^{-1}, corresponding to the 50th percentile of the rate probability density function. The rate factor uncertainty, f.u., is obtained from the 16th and 84th percentiles (see the text). Values for $T > 1$ GK, shown in italics, are adopted from Descouvemont et al. (2004).

Table 4. The ^{2}H(t,α)n Data of Jarmie et al. (1984).

E_{cm} [a] (keV)	$S \pm \Delta S_{\rm stat}$ [b] (MeVb)	E_{cm} [a] (keV)	$S \pm \Delta S_{\rm stat}$ [b] (MeVb)
4.992	12.63±0.58	27.996	20.70±0.09
5.990	13.48±0.39	31.998	22.19±0.11
6.990	12.83±0.40	36.001	24.02±0.11
7.990	13.43±0.27	40.004	25.28±0.14
9.989	13.92±0.14	42.005	26.00±0.12
11.989	14.32±0.10	44.007	26.30±0.14
15.990	15.81±0.13	46.009	26.74±0.13
19.992	17.35±0.09	46.809	26.64±0.14
23.994	18.87±0.08		

[a] Total uncertainty varies from ±2.4 eV at E_{cm} = 5 keV to ±6.4 eV at E_{cm} = 47 keV.

[b] Systematic uncertainty: 1.26%.

Table 5. The ^{3}H(d,α)n data of Brown et al. (1987).

E_{cm} [a] (keV)	$S_{\rm rel} \pm \Delta S_{\rm stat}$ [b] (MeVb)	E_{cm} [a] (keV)	$S_{\rm rel} \pm \Delta S_{\rm stat}$ [b] (MeVb)
47.948	26.48±0.21	59.941	24.33±0.19
50.947	26.84±0.21	62.941	23.44±0.19
53.942	25.89±0.21	65.941	22.02±0.18
56.942	25.50±0.20	69.541	20.34±0.16

[a] Total uncertainty of center-of-mass energy is ±9 eV.

[b] The values reported in Brown et al. (1987) were normalized relative to the data of Jarmie et al. (1984), listed in Table 4.

Table 6. The ^{2}H(t,α)n Data of Kobzev et al. (1966).

$E_{cm} \pm \Delta E_{cm}$ [a] (keV)	$S \pm \Delta S_{\rm stat}$ [b] (MeVb)	$E_{cm} \pm \Delta E_{cm}$ [a] (keV)	$S \pm \Delta S_{\rm stat}$ [b] (MeVb)
46.0±1.2	25.93±0.52	132.0±2.6	5.23±0.10
48.0±1.2	25.96±0.52	136.0±2.7	4.89±0.10
52.0±1.3	25.76±0.52	140.0±2.8	4.60±0.09
56.0±1.4	25.28±0.51	144.0±2.9	4.32±0.09
60.0±1.5	24.77±0.50	148.0±3.0	4.11±0.08
64.0±1.3	23.66±0.47	152.0±3.0	3.88±0.08
66.0±1.3	22.85±0.46	156.0±3.1	3.69±0.07
68.0±1.4	21.89±0.44	160.0±3.2	3.50±0.07
72.0±1.4	19.98±0.40	164.0±3.3	3.32±0.08
76.0±1.5	18.14±0.36	168.0±3.4	3.15±0.08
80.0±1.6	16.53±0.33	176.0±3.5	2.84±0.07
84.0±1.7	15.01±0.30	184.0±3.7	2.62±0.07
88.0±1.8	13.65±0.27	192.0±3.8	2.42±0.06
92.0±1.8	12.50±0.25	200.0±4.0	2.26±0.06
96.0±1.9	11.41±0.23	208.0±4.2	2.13±0.05
100.0±2.0	10.45±0.21	216.0±4.3	2.00±0.05
104.0±2.1	9.59±0.19	224.0±4.5	1.89±0.05
108.0±2.2	8.76±0.18	232.0±4.6	1.79±0.04
112.0±2.2	7.98±0.16	240.0±4.8	1.69±0.04
116.0±2.3	7.28±0.15	248.2±5.0	1.60±0.04
120.0±2.4	6.65±0.13	256.2±5.1	1.51±0.04
124.0±2.5	6.08±0.12	264.3±5.3	1.44±0.04
128.0±2.6	5.61±0.11		

[a] Triton laboratory energies have a 2.5% accuracy in the range 115 − 150 keV, and a 2% accuracy in the range 150 − 1200 keV (see text).

[b] Assumed systematic uncertainty: 2.5% (see text).

Table 7. The ^{3}H(d,n)^{4}He Data of Arnold et al. (1953).

E_{cm} [a] (keV)	$S \pm \Delta S_{\rm stat}$ [b] (MeVb)	E_{cm} [a] (keV)	$S \pm \Delta S_{\rm stat}$ [b] (MeVb)
8.98	13.340±0.026	31.52	22.695±0.023
9.32	13.703±0.027	35.36	24.314±0.024
9.47	13.508±0.027	35.38	24.589±0.024
9.52	13.600±0.027	37.00	24.967±0.025
11.95	14.068±0.028	37.16	25.184±0.025
11.99	13.849±0.028	41.23	26.600±0.027
12.03	13.680±0.027	41.25	26.514±0.026
12.81	14.302±0.029	43.29	27.067±0.027
12.83	14.957±0.030	42.49	26.847±0.027
14.48	14.939±0.030	46.61	27.466±0.027
14.68	15.753±0.031	46.64	27.365±0.027
14.89	15.448±0.030	46.65	27.489±0.027
18.33	16.921±0.034	47.22	27.505±0.027
18.35	16.989±0.032	47.25	27.542±0.027
19.92	17.249±0.034	52.80	26.975±0.027
20.27	17.721±0.035	52.83	27.085±0.027
23.95	18.969±0.038	58.66	25.621±0.025
23.97	18.366±0.036	58.68	25.669±0.026
25.17	20.718±0.021	61.39	24.593±0.024
25.26	20.755±0.021	61.43	24.492±0.024
25.32	19.969±0.020	64.51	23.071±0.023
25.66	19.920±0.020	64.54	23.157±0.023
25.72	20.596±0.020	67.37	22.002±0.022
26.09	20.277±0.020	67.39	21.951±0.022
26.38	20.525±0.020	70.39	20.445±0.020
29.95	21.766±0.022	70.44	20.227±0.020
31.16	22.749±0.023		

[a] Total uncertainty of center-of-mass energy is about ±75 eV (see text).

[b] Adopted systematic uncertainty: 2.0% (see text).

Table 8. The ^{3}H(d,n)^{4}He Data of Conner et al. (1952).

E_{cm} [a] (keV)	$S \pm \Delta S_{\rm stat}$ [b] (MeVb)	E_{cm} [a] (keV)	$S \pm \Delta S_{\rm stat}$ [b] (MeVb)
12.42	13.23±0.13	65.40	23.43±0.23
15.48	15.17±0.15	66.60	22.90±0.23
18.60	15.79±0.16	69.00	21.82±0.22
20.70	17.33±0.17	75.00	19.23±0.20
21.78	17.38±0.17	80.40	16.97±0.17
24.90	18.23±0.18	81.60	16.60±0.17
28.02	19.70±0.20	85.80	14.96±0.15
29.10	20.13±0.20	87.60	14.27±0.14
31.20	21.80±0.22	91.80	12.90±0.13
33.24	22.91±0.23	93.60	12.33±0.12
34.26	21.59±0.21	97.20	11.02±0.11
37.38	23.80±0.24	100.2	10.63±0.11
40.50	25.31±0.25	103.8	9.91±0.10
41.58	25.72±0.26	109.8	8.99±0.09
43.68	25.93±0.26	123.0	6.79±0.07
45.72	25.90±0.26	136.2	5.44±0.05
46.80	25.44±0.25	150.6	4.43±0.04
49.98	26.83±0.27	165.6	3.55±0.04
54.18	25.53±0.26	181.2	2.89±0.03
56.22	26.60±0.27	197.4	2.51±0.03
58.26	25.89±0.26	214.2	2.16±0.02
62.40	24.61±0.25		

[b] We assumed that the uncertainty varies from ±60 eV at 12.4 keV to ±600 eV at 214 keV center-of-mass energy (see text).

[b] Adopted systematic uncertainty: 1.8% (see text).